

Structure determination to calculate nonlinear optical coefficients in a class of organic material

I. G. Voigt-Martin,* Gao Li, U. Kolb, H. Kothe, and A. V. Yakimanski†

Institut für Physikalische Chemie der Johannes Gutenberg Universität, Jakob-Welder-Weg 11, D-55099 Mainz, Germany

A. V. Tenkovtsev

Institute of Macromolecular Compounds of Russian Academy of Sciences, Bolshoi prospect 31, 199004 St.-Petersburg, Russia

C. Gilmore

Department of Chemistry, University of Glasgow, Glasgow G 12 8QQ, Scotland, United Kingdom

(Received 3 August 1998)

A class of molecules with intramolecular two-dimensional charge transfer upon excitation has been synthesized. It is expected that these materials should be prospective candidates for nonlinear optical (NLO) applications such as second harmonic (SHG) generation. In order to optimize the macroscopic NLO properties of the compounds, it is necessary to relate their first hyperpolarizability tensors at a molecular level to those at a crystal bulk level. This requires a complete structure determination and refinement. However, the growth of sufficiently large single crystals, which are needed for structural analysis and refinement by x-ray methods, is a time-consuming and sometimes impossible task. Even larger crystals are required for NLO measurements. Single crystals of a considerably smaller size may be effectively used for complete structural analysis by electron diffraction combined with simulation methods. In addition the structure has been confirmed structure solution from electron diffraction intensities using maximum entropy and log likelihood methods. When the crystal structure of a given compound is known, its NLO properties may be estimated using quantum-mechanical methods for calculation of the molecular nonlinearity tensor and these may be related to the macroscopic coefficients of the crystalline nonlinearity tensor. In the present work, both *ab initio* and semi-empirical quantum-mechanical calculations were employed. [S0163-1829(99)09305-4]

I. INTRODUCTION

The motivation for this work has been to reach a better understanding of the relationship between the structure of organic molecular crystals and their second order nonlinear optical properties. The further aim is to find a more specifically directed route towards the synthesis of molecules with the required molecular architecture. This approach required close collaboration between specialists in organic chemistry, physics as well as electron microscopy and can be described by the term crystal engineering.

The effect which is observed in second order NLO is that of frequency doubling, or second harmonic generation (SHG). The physical effect which can be measured is the optical susceptibility χ_{IJK} in crystallographic coordinates I, J, K . In our examples, an incoming beam of infrared light ($\lambda = 1047$ nm) emerges as green light ($\lambda = 523.5$ nm). Prac-

tical applications are found in optoelectronic devices and are therefore candidates for future communication systems. Organic materials have SHG efficiencies which are greater than those of classical inorganic materials like lithium niobate or potassium dihydrogen phosphate but poorer mechanical properties. However organic compounds offer much more scope for deliberately tailoring both electronic and crystallographic properties as well as offering the possibility of processing in different geometries.

During the past decade π -conjugated systems with effectively one-dimensional charge transfer have been used for nonlinear optical applications.¹ The molecular property which is responsible for second harmonic generation is the quadratic hyperpolarizability tensor β_{ijk} expressed in molecular coordinates i, j, k . The relationship between microscopic and macroscopic parameters is given by

$$\chi_{IJK}(-2\omega; \omega_1, \omega_2) = (N/V) \left[f_I(\omega) f_J(\omega) f_K(\omega) \sum \sum \cos \theta_{Ii} \cos \theta_{Jj} \cos \theta_{Kk} \beta_{ijk}(-2\omega, \omega_1, \omega_2) \right], \quad (1)$$

where V is the unit cell volume, N is the number of molecules per unit cell, $f_I(\omega)$ are local field factors at frequency ω for the I direction in the crystal, etc., and the θ_{Ii} are the rotation angles relating microscopic and macroscopic axes. The local field factors $f_I(\omega)$ depend on the linear polarizabil-

ity term α_{II} , which is related to the refractive indices of the crystal. The macroscopic susceptibility coefficients d_{IJK} which are actually measured in an experiment are directly related to χ_{IJK} by a factor of 0.5 and to the direction of the incoming and outgoing beams with respect to the crystal

axes. They depend on the crystal symmetry, the precise orientation of the molecule with respect to the crystal axes and the conformation of the molecule. It will be shown how all this information can be obtained by a combination of electron crystallography with quantum-mechanical calculations.

In linear systems there is a fundamental theoretical limit for the coefficient of transformation of the molecular nonlinearity into crystalline nonlinearity. Depending on the crystal space group and the orientation of the molecules in a crystal cell with respect to the crystal axes, this coefficient has a maximum value of 38% at phase-matching with respect to the direction of the fundamental beam propagation.² Therefore the search for NLO-active molecules with, at least, two-dimensional intra-molecular charge transfer is of both theoretical and practical interest. For second harmonic generation such systems must crystallize in a non-centrosymmetric space group.

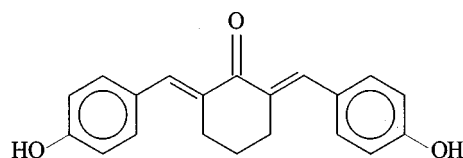
While the molecular quadratic hyperpolarizability tensor, β_{ijk} , in linear systems has a dominant vectorial contribution, in nonlinear molecules the charge transfer is, at least, two-dimensional in character. Thus the β tensor may contain both the diagonal components β_{iii} as well as off-diagonal ones.³ In the crystalline state, individual coefficients of the molecular β tensor can be determined provided the molecular conformation in the crystal is known precisely. The relationships between the β_{ijk} values and the crystalline-per-molecule nonlinear tensor coefficients, b_{IJK} , have been treated in a fundamental paper by Zyss.²

Frequently it is not possible to grow large single crystals for a full x-ray structure analysis, so that the development of electron crystallography, requiring single crystals which need only be ca. 100 Å thick and several hundred Å long, becomes mandatory. We have been able to solve several unknown structures using two new methods, namely, simulation of electron diffraction patterns from suitable model structures⁴⁻⁸ and maximum entropy combined with log-likelihood evaluation.⁹⁻¹¹

In this paper we study the molecular and crystallographic parameters relevant for second harmonic generation in a two-dimensional molecule. The structural data were used to calculate the angular parameters of the molecular orientations in the cell and to relate the crystalline nonlinear tensor coefficients b_{IJK} to the components of the molecular β tensor. An estimation of the refractive indices of the crystals along the crystal axes and the corresponding local-field factors, relating the b_{IJK} coefficients to the experimentally measurable macroscopic d_{IJK} coefficients, was performed based on the calculated molecular linear polarizability tensor α , reduced to the crystal axes frame. For the calculations of molecular α -tensor, both semiempirical quantum-mechanical PM-3 (Ref. 12) and *ab initio* calculations were used. Molecular β -tensor was calculated by the semiempirical PM-3 method only. On the basis of these calculations predictions can be made regarding the suitability of a specific molecule for SHG applications.

II. SAMPLE

Single crystals of 2,6-bis(4-hydroxy-benzylidene)-cyclohexanone (BHBC) were grown from a 1% solution in ethanol. The molecular architecture is indicated below.



Chemical characterization data

Melting point: 291 °C (crystallized from ethanol).		
Elemental analysis	H	C
calculated, %	5.30	78,92
found, %	5.30	78,28

Maximum wavelength of UV absorption: 376 nm (in ethanol). ¹H NMR shifts: singlet 1.85 ppm (2H), multiplet 2.8 ppm (4H), doublet 6.82 ppm (4H), doublet 7.20 ppm (4H), singlet 7.55 ppm (2H), singlet 10.0 ppm (2H).

III. METHODS

A. Quantum-mechanical calculations

In order to generate a minimum energy gas phase conformation of the molecule, both semiempirical and *ab initio* quantum-mechanical calculations can be performed. The application of the semiempirical PM-3 method,¹² which is implemented into the MOPAC program package,¹³ to simulations combined with electron diffraction analysis has been described in several papers previously.^{5,8,10-11}

In this work, the *ab initio* density functional theory (DFT) approach¹⁴ implemented into the TURBOMOLE program package¹⁵ was also used to calculate the equilibrium gas phase conformation of the BHBC molecule. For the DFT-geometry optimization, the Becke-Perdew 86 energy functional¹⁶ and the TURBOMOLE split-valence (7s4p)/[3s2p] basis,¹⁷ augmented with one *d*-polarization function for carbon (*d*-exponent 0.8) and oxygen (*d*-exponent: 1.2) and double- ζ (4s)/[2s] basis set for hydrogen, were used. This would enable one to correct for possible inaccuracies of a semiempirical description of the conformation-determining balance between the π conjugation and steric repulsion factors.

While semiempirical methods within the MOPAC program often produce good results for static polarizabilities,¹⁸ it cannot be used to calculate frequency-dependent polarizability α tensors needed for estimation of frequency-dependent local-field factors $f_l(\omega)$ entering Eq. (1). Earlier,⁸ we used PM-3 static values of α -tensor components to calculate d_{IJK} values of molecules similar to BHBC and got reasonable estimations. This approach was also reproduced here. However, in order to estimate the error in the calculated d_{IJK} values due to using frequency-independent f_l values in Eq. (1), both static and frequency-dependent α tensors were also calculated by *ab initio* method using the TURBOMOLE program. The calculations were performed with the 6-31G basis set augmented with polarization *p* and *d* functions at hydrogen and nonhydrogen atoms, respectively, and with diffuse *s* functions at all atoms. This basis set is referred to as 6-31G(+*sp*, +*sd*), which is specially optimized for molecular polarizability calculations.¹⁹

For both semiempirical and *ab initio* calculations of the polarizability and first hyperpolarizability tensor components, the molecular conformation corresponding to the crystal geometry was used.

Equilibrium gas phase BHBC geometries and molecular polarizabilities predicted by semiempirical and *ab initio* calculations are compared in order to demonstrate the areas in which the more simple semiempirical calculations are not sufficiently accurate.

B. Structure determination

Single crystal electron diffraction data were obtained with a Philips transmission electron microscope, using a rotation-tilt holder in order to obtain diffraction patterns from suitable crystallographic zones and a low dose unit to reduce beam damage. The maximum tilt angle is 60° , so that there is a cone of 30° in any specific crystal which contains zones inaccessible to electron diffraction. If other crystals can be found having a different orientation with respect to the electron beam, this information can be supplemented. X-ray powder diffraction data were also used to increase the accuracy of the lattice spacings obtained from the electron diffractograms and to obtain information regarding dynamical or secondary scattering.¹¹ Peaks which appear in electron diffraction but are absent in the x-ray diffractograms are strong indications of dynamical scattering. For x-ray powder diffraction investigations, a Siemens D-500 diffractometer in the $\Theta/2\Theta$ reflection mode (Cu $K\alpha$ -radiation with $\lambda = 1.542 \text{ \AA}$) was used.

With regard to the electron diffraction analysis it should be stated that a degree of accuracy is required which goes far beyond that required for a standard determination of the unit cell. Both for the simulations and the maximum entropy calculations we need an accurate intensity determination from many different projections. The difficulty here is not only in recording the data correctly but also the more fundamental problem that intensity changes are induced by secondary and dynamic scattering.^{20,21} After the space group forbidden reflections have been identified, the initial model is calculated by using the kinematic approximation. In the refinement stage, dynamical scattering effects must be calculated.

For subsequent quantitative analysis it is essential to produce both tilt and exposure series.^{11,22} Frequently, the forbidden reflections are revealed as such during tilting. In this laboratory tilting is always performed about specific axes containing strong reflections. If the structure is unknown initially, this makes it much easier to identify zones and to determine angles between planes. In addition, the common axis can then be used for calibration purposes.

From the series of electron diffraction patterns, several space groups are usually possible and can only be reduced to the unique one in the course of further refinement.

C. Quantifying electron diffraction patterns

Electron diffraction data were scanned with a Nikon LS 4500 AF scanner at a resolution of 3000 d.p.i. and transferred to a PC for quantifying using the ELD software.²³ Recently there have been considerable improvements in this program so that more accurate data can be obtained. It is essential to ensure that ELD is evaluating the intensities in

saturation correctly by studying exposure series. It is also essential to calibrate the film emulsion. This can now be done quite quickly with the appropriate software.²² It is expected that the accuracy of intensity data can be considerably improved by the use of an on-line slow scan CCD camera with a larger dynamic range.

The quantitative values are first compared with those expected kinematically from the initial model (see Sec. III D). Each zone is inspected individually for signs of secondary or dynamical scattering. The quality of the data as well as the accuracy of the model are assessed by the R value, defined as in x-ray scattering as

$$R = \frac{\sum_{hkl} ||F_0| - |F_c||}{\sum_{hkl} |F_0|}.$$

D. Simulation of diffraction patterns

On the basis of cell parameters and space group calculated from electron diffraction pattern and x-ray powder data a first model was built up in CERIOUS 2.0. Initially, the BHBC molecule, with gas phase conformation obtained from quantum-mechanical calculations, was placed into the unit cell.

Packing energy calculations were performed using the crystal packer module of CERIOUS 2.0. This is a force field approach with the limitations which we have pointed out previously.^{7(a)} For the BHBC molecule studied here, the optimal gas phase conformation of its cyclohexanone moiety can differ from an exact crystal state conformation. This difference cannot be removed by the Crystal Packer because it does not optimize subrotations within cyclic molecular fragments. Also, the effect of intermolecular H-bonds between BHBC molecules in the crystal state cannot be taken into account by gas phase calculations of an isolated molecule.

Usually, PM-3 gas phase calculations reproduce bond geometry (bond lengths and bond angles) quite reasonably. However, in some situations, *ab initio* calculations lead to a considerably different molecular geometry. For the molecule discussed here, the latter geometry was much more favorable regarding molecular packing in the unit cell and was therefore used for the initial model.

In order to avoid positive packing energies and to provide the most favorable intermolecular H-bonding, slight adjustments to torsional angles were necessary.^{4,5,9,10}

Electron diffraction patterns from all zones and the x-ray powder pattern were simulated and refined against experimental data. After several circles between minimization of the packing energy and comparison with diffraction data, the model structure was obtained, giving details about the adjusted molecular conformation and arrangement in the unit cell. The linear polarizability and first hyperpolarizability tensor components for the asymmetric unit of the unit cell were then calculated for the crystal state molecular conformation.

E. The maximum entropy method of solving crystal structures

The solution of structures of this complexity from electron diffraction data is difficult. In the case of small molecule x-ray data, direct methods are usually employed, and these work in a more or less routine manner. However, they require that reciprocal space is fully sampled to a resolution of

at least 1.1 Å, and that the data are free from significant systematic error. In the case of electron diffraction the missing cone problem, associated sampling difficulties and the presence of dynamical scattering effects mean these traditional methods are usually impossible and this was the case here. There are a few reflections in this data set with a resolution of ca. 1 Å, but, in general, the resolution is closer to 1.5 Å and, despite extensive sampling, the data set is incomplete. The solution technique used instead of direct methods was the maximum entropy (ME) method combined with likelihood evaluation. This formalism was first proposed by Bricogne,²⁴ and subsequently developed by Bricogne and Gilmore^{25,26} into a technique for use with small molecules including data from powder,²⁷ surface diffraction,²⁸ electron diffraction,^{9–11,29} and protein crystallography.³⁰ A review of the maximum entropy method in crystallography can be found in Ref. 31.

The ME method has been described in detail elsewhere and will only be outlined here.

(1) Unitary structure factor magnitudes $|U_h|^{\text{obs}}$ and their associated standard deviations $\sigma_h = \sigma |U_h|^{\text{obs}}$ are computed from the observed structure factors $|F_h|^{\text{obs}}$ using the Wilson normalization method and electron scattering factors to obtain an estimate of an overall isotropic thermal parameter, B , and a scale factor that puts the observed structure factor on an absolute scale.³² Each U magnitude has an associated phase angle φ_h , and the phase angles for the strongest amplitudes only are required.

(2) There are well-defined rules governing origin and enantiomorph definition which allow some phases to be assigned *ab initio* according to the space group, and used as a starting point in phase determination. This usually involves a maximum of four such phases. In the ME method, the reflections so phased comprise the basis set $\{H\}$ while the much larger disjoint set, the nonbasis set, of unphased amplitudes is $\{K\}$. There is a third set of reflections $\{U\}$, disjoint to both $\{H\}$ and $\{K\}$, of reflections, which are unmeasured. The phased reflections, both amplitude and phase, so selected are used as constraints in a constrained entropy maximization calculation to compute a maximum entropy map $q^{\text{ME}}(x)$ which satisfies the following criteria.

(a) It is optimally unbiased by virtue of having maximum entropy, i.e., it does not assume that the non-basis-set coefficients have zero amplitude.

(b) The Fourier transform of $q^{\text{ME}}(x)$ generates $|U_h^{\text{ME}}|$ and φ_h^{ME} and reproduces the observed U magnitudes $|U_h|^{\text{obs}}$ and their associated phases belonging to $\{H\}$ to within experimental error.

(c) The Fourier transform of $q^{\text{ME}}(x)$ generates estimates of amplitudes and phases for non-basis-set reflections in both $\{K\}$ and $\{U\}$ thus generating new phase information *via* a process of extrapolation. In the early stages of phasing when only the origin and enantiomorph reflections have been assigned, the extrapolation is weak.

(3) To overcome the problem of weak extrapolation, unphased reflections are now added to the starting set. Since their phases are unknown, they are given permuted values, which span the phase space, thus giving rise to a multisolution environment. To do this, a few reflections with large associated U magnitudes are selected using an algorithm of optimal second neighborhood enlargement.²⁵ For centric re-

flections both possible values of the phase angle are used for phase angle permutation, e.g., $0, \pi$, while for acentric reflections quadrant permutation is used with unknown angles taking the 4 values $\pm\pi/4, \pm3\pi/4$. Alternatively suitable binary error-correcting codes can be employed.^{33–35} A constrained entropy maximization for each possible phase permutation is now carried out. Each of these phase choices is described as a node on a phasing tree, where the first level of the tree is the root node defined by the origin fixing reflections, and the second level is defined by the sets generated by the phase permutation process.

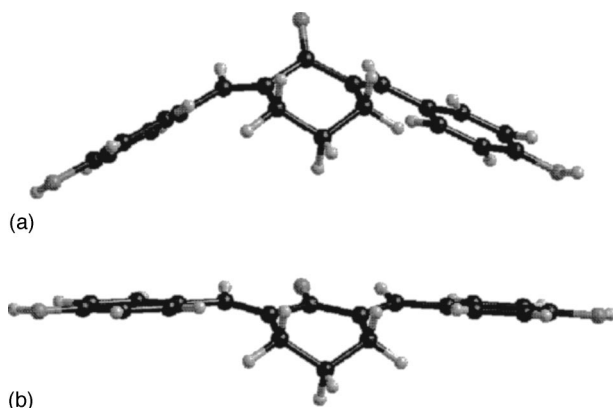
The use of binary error-correcting codes here needs further amplification. In the method of phase permutation, n_c centric reflections are given both possible phase values, e.g., $0, \pi$ (or $\pm\pi/2$), and each of the n_a acentric reflections is assigned a quadrant by assigning the possible values $\pm\pi/4, \pm3\pi/4$. This is a full factorial design generating $2^{n_c} 4^{n_a} = 2^{n_c + 2n_a}$ phase choices, and it can be seen that this soon becomes a combinatorial explosion, e.g., permuting the phases of 7 acentric reflections along with 3 centric ones would give 131 072 phase combinations each of which needs to be subjected to the computationally intensive task of constrained entropy maximization. Error-correcting codes (ECCs) represent an alternative approach.^{33–35} (For a standard text on the subject see Ref. 36 or the simpler Ref. 37.) Certain ECCs contain a suitable experimental design that balances both the main reflection phases and the interactions between them, as well as covering the phase space with optimum efficiency and can be used as a source of highly efficient phase permutation. In this work we have used the Golay^{24,12,8} code³⁸ which produces 4096 phase combinations or nodes instead of $2^{24} = 16\,777\,216$. One of these choices will have a maximum of 4 incorrect phases, and, in general, this level of error is not too great to prevent identification of the molecular features in the potential maps. The gain in efficiency here is exceptional, and the code links to the extraordinary Leech lattice and the packing of spheres in 24 dimensions in which each sphere has a kissing number of 196 560, and is the densest packing known in any dimension.³⁹

To use binary codes for phase permutation is straightforward. For centric phases the digit ‘‘0’’ represents one possible choice, and ‘‘1’’ the alternative, e.g., for a phase restricted to 0 or π , 0 represents a zero degree phase angle and 1 an angle of π . In the acentric case two bits are used to assign the quadrant of the phase; one bit describes the sign of the real part of the phase and the second the imaginary part i.e., $(0,0) = \pi/4, (1,0) = 3\pi/4, (1,1) = 5\pi/4$ and $(0,1) = 7\pi/4$.

(4) To judge which phase sets are the most probable is done using likelihood estimation.²⁵ For each centric extrapolated, non-basis-set reflection $k \in K$, the likelihood measure, in its diagonal approximation, can be written

$$\Lambda_k = \left[\frac{2}{\pi(\varepsilon_k \Sigma + \sigma_k^2)} \right]^{1/2} \times \exp \left\{ -\frac{1}{2} \frac{(|U_k|^{\text{obs}})^2 + |U_k^{\text{ME}}|^2}{\varepsilon_k \Sigma + \sigma_k^2} \right\} \cosh \left(\frac{|U_k|^{\text{obs}} |U_k^{\text{ME}}|}{\varepsilon_k \Sigma + \sigma_k^2} \right). \quad (2)$$

Σ is a refinable measure of unit cell contents ($\Sigma \approx 1/2N$) for N atoms, assumed equal, in the unit cell, and ε_k is the sta-



A) semi-empirical PM-3 method b) DFT-*ab initio* approach

$$\begin{aligned}\alpha_{xx} &= 44.9 \text{ \AA}^2 \\ \alpha_{yy} &= 112.7 \text{ \AA}^2 \\ \alpha_{zz} &= 17.4 \text{ \AA}^2\end{aligned}$$

$$\begin{aligned}\alpha_{xx} &= 55.2 \text{ \AA}^2 \\ \alpha_{yy} &= 131.0 \text{ \AA}^2 \\ \alpha_{zz} &= 40.6 \text{ \AA}^2\end{aligned}$$

FIG. 1. Gas phase conformation of the BHBC molecule calculated by the semiempirical PM-3 method (a) and the DFT-*ab initio* approach (b).

tistical weight arising from crystallographic point group symmetry. Equation (2) measures the agreement between $|U_k^{\text{obs}}|$ and $|U_k^{\text{ME}}|$, having a maximum value when they are equal, and thus tells us how well we have predicted the amplitudes which were not included as constraints in the entropy maximization. There is a similar expression for acentric reflections where the Bessel function I_0 replaces the hyperbolic cosine term in (2), and there is some small adjustment to the arguments.

As in traditional likelihood analysis, a null hypothesis is defined. Here this is the situation of zero extrapolation, $|U_k^{\text{ME}}| = 0$, and defines Λ_k^0 which describes the effect on no extrapolation, and defines a likelihood baseline. The global log-likelihood gain (LLG) for a node n is then

$$\text{LLG}_n = \sum_{k \in K} \ln \frac{\Lambda_k}{\Lambda_k^0}. \quad (3)$$

The LLG should be largest when the phase choices made for a given node lead to extrapolated amplitudes for the unphased reflections which best agree with the observed ones, and indeed, it has proved to be a powerful figure of merit. However, rather than just choose those phase sets with high associated LLG, which can be an error prone process, tests of significance based on the student t test are used. These are not described here, but are discussed in detail in Refs. 28 and 40. The top eight nodes from this analysis are kept and their associated maps (see below) are calculated. If a recognizable part of the structure appears then traditional crystallographic methods of model building and refinement are employed to complete it, if not, then the 8 nodes which have been retained act as root nodes for another level of permutation and entropy maximization, thus building the third level of the phasing tree. Further levels may be needed in difficult cases.

(5) The function $q^{\text{ME}}(\underline{x})$ is a probability distribution, and not a potential map in the traditional sense (although its

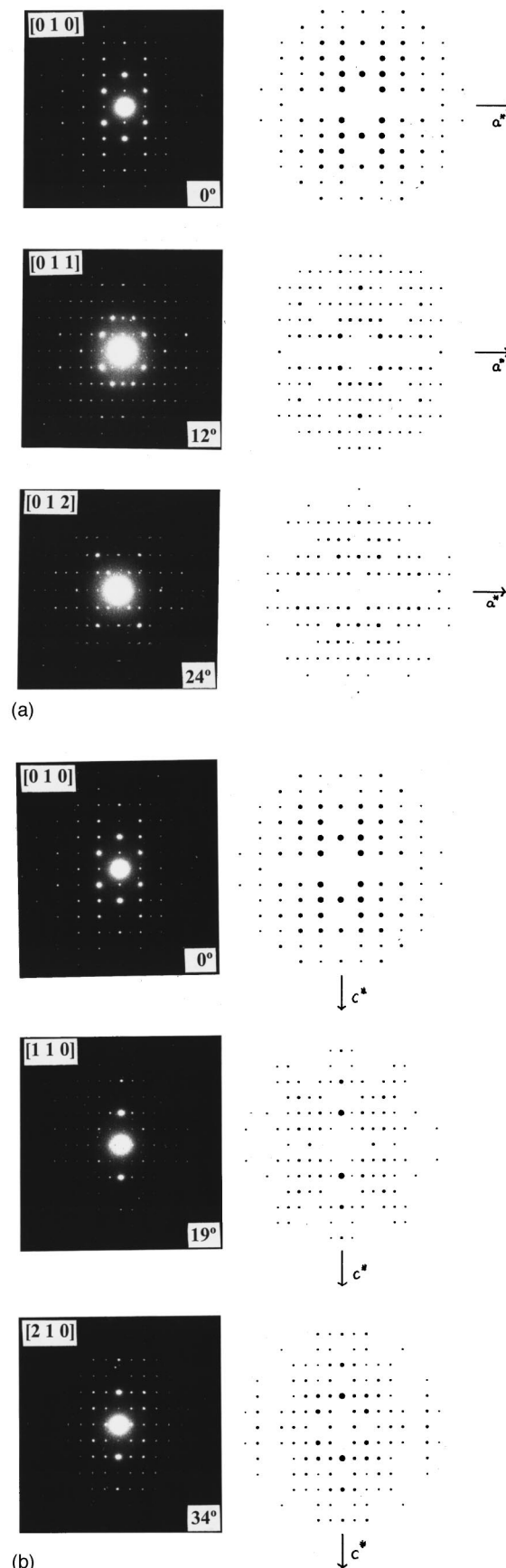


FIG. 2. Tilting series about a^* axis (a) and c^* axis (b) obtained from BHBC crystals (LHS experimental electron diffraction patterns; RHS simulated diffraction patterns).

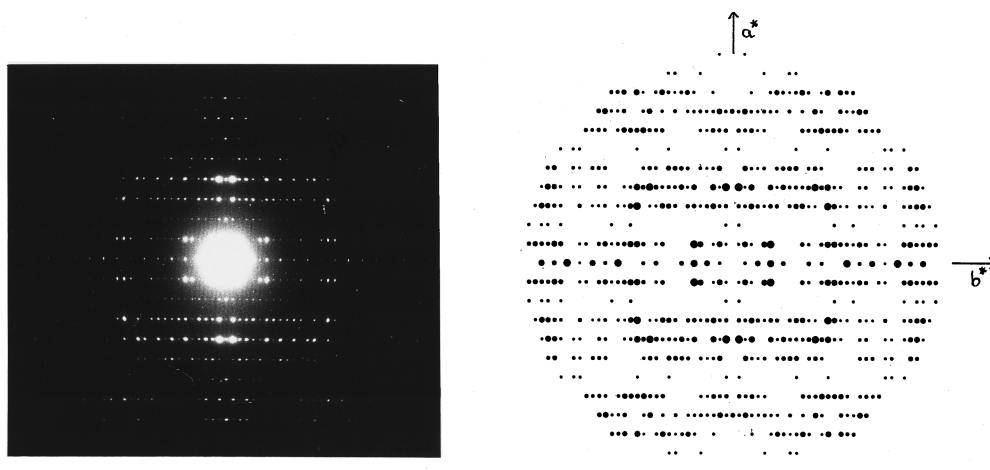


FIG. 3. [001] zone of BHBC. (LHS experimental electron diffraction patterns; RHS simulated diffraction patterns.)

peaks do correspond to atom positions). The maps examined in the ME formalism are centroid maps,²⁵ which are computed as Sim filtered⁴¹ U -maps where the basis set reflections contribute with full weight, and the extrapolated reflections are given coefficients computed via

$$|U_{\vec{k}}|^{\text{obs}} \tanh(X_{\vec{k}}) \exp(i\varphi_{\vec{k}}^{\text{ME}}), \quad (4)$$

where

$$X_{\vec{k}} = (N/\varepsilon_{\vec{k}}) |U_{\vec{k}}|^{\text{obs}} |U_{\vec{h}}^{\text{ME}}|. \quad (5)$$

The ME method does not require complete data to a 1.1 Å; it is stable irrespective of resolution, and robust with respect to data measurement errors. The MICE computer program is a practical implementation of the formalism (see, for example, Refs. 30 and 42), and is used here for the solution of the crystal structure of the NLO material. For an example of the use of the Golay code in conjunction with ME and electron diffraction see Ref. 43.

IV. RESULTS

A. Quantum-mechanical calculations of the molecular gas phase conformation

The lowest energy gas phase conformations of the BHBC molecule calculated by the PM-3 and DFT-*ab initio* methods are presented in Figs. 1(a) and 1(b), respectively.

As is shown in Fig. 1(a), the PM-3 method predicts a folded equilibrium gas phase conformation. This seems unlikely for the crystal state because the crystal cell parameters (Sec. IV B) imply an extended BHBC conformation. Precisely this latter type of gas phase conformation was found by DFT-*ab initio* calculations [Fig. 1(b)]. The reason of the artifact by PM-3 is, probably, an underestimation of the π -conjugation, favoring more flat and extended conformation, by the semiempirical method.

B. Structure determination

1. NLO measurements

Optical measurements on BHBC using the method described previously⁴⁴ gave a rather low intensity of SHG green light. This result is an indication that the unit cell is

noncentrosymmetric but that either the individual components of the hyperpolarizability tensor are very small or that many components mutually cancel.

2. Determination of space group and cell parameters

Electron diffraction patterns are taken from zone [010] [Figs. 2(a) and 2(b)] with corresponding tilt series and from zone [001] (Fig. 3), whereas the x-ray powder pattern is shown in Fig. 4.

The basic zone [0 1 0] has a net angle of 90° and d -spacings of the (1 0 0) and (0 0 1) reflections equal to 11.7 Å and 7.6 Å, respectively. When tilting about the a^* axis [Fig. 2(a)], zonal diffraction patterns appear at $\pm 12^\circ$ and $\pm 24^\circ$ with an accuracy of $\pm 1^\circ$ after averaging over 5 crystals. When tilting about the c^* axis [Fig. 2(b)], zones appear at $\pm 19^\circ$ and $\pm 34^\circ$. Tilting to the left and right directions from the basic zone gives identical diffraction patterns. This implies that the c^* axis is perpendicular to the a^*b^* plane,

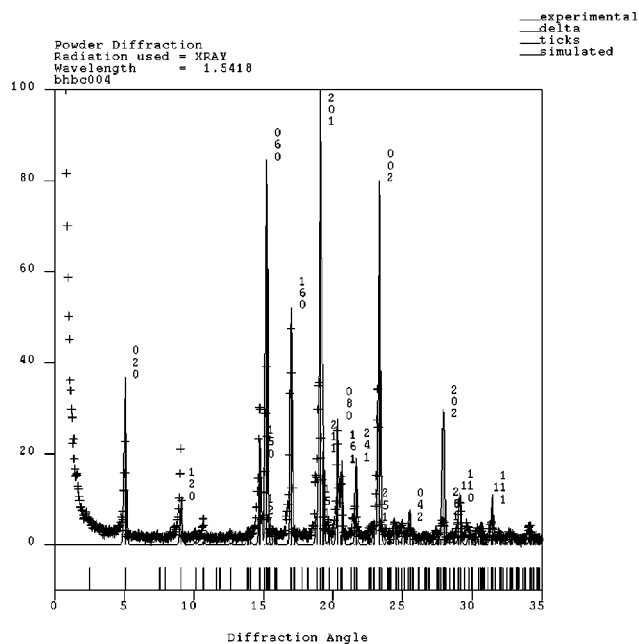


FIG. 4. Experimental x-ray powder pattern and simulated data of BHBC.

and the a^* axis is perpendicular to the b^*c^* plane. Therefore the unit cell metric indicates an orthorhombic unit cell.

As in x-ray diffraction, the space group can be obtained by checking systematic absences in the diffraction patterns from different projections. Considering the extinction conditions for the BHBC electron diffraction patterns, it was found that the odd ($h\ 0\ 0$) and ($h\ 0\ 1$) reflections were systematically much weaker than the even ones. The appear-

ance of forbidden reflections in electron diffraction patterns due to secondary scattering and/or dynamical effects is well known and often leads to characteristically weak reflections in organic crystals. This observation indicates that there are probably extinctions for ($h\ 0\ 0$) and ($0\ 0\ 1$) reflections, when h or l equal to $2n+1$, respectively. Applying the same analysis for all 6 different zones from tilting and basic zone [001], the allowed reflections for BHBC are as follows:

Allowed reactions	Symmetry element	Used zones
$h\ 0\ 1$: ($h=2n$) and $h\ 0\ 0$: ($h=2n$)	a glide plane $\perp b$	[0 1 0], [0 1 1], [0 1 2], [1 1 0], [2 1 0] (Fig. 2)
$0\ k\ 0$: ($k=2n$)	n glide plane $\perp a$	[0 0 1] (Fig. 3)
$0\ k\ 1$: ($1=2n$) and $0\ 0\ 1$: ($k+1=2n$)	n glide plane $\perp a$	[0 1 0], [0 1 1], [0 1 2] [Fig. 2(a)]
$h\ k\ 0$ and $h\ k\ 1$: no conditions		

The two possible orthorhombic space groups, consistent with these extinction conditions and in agreement with the x-ray powder pattern, are the centrosymmetric space group $Pnam$ (Pnam No. 62) and its corresponding noncentrosymmetric space group $Pna2_1$ (No. 33 International Tables of Crystallography). Since the powder crystals show second harmonic generation (SHG), the only possible space group is $Pna2_1$ with cell parameters:

$$a = 11.70 \text{ \AA},$$

$$b = 34.89 \text{ \AA},$$

$$c = 7.64 \text{ \AA}.$$

3. Packing considerations

For the calculation of crystal NLO properties the orientation of the molecule with respect to the crystal axes must be determined.

According to the crystal density it is obvious that the asymmetric unit for space group $Pna2_1$ contains two independent BHBC molecules in order to give a reasonable density. Moreover, the b value is close to the double length of the molecule in its extended conformation [Fig. 1(b)]. This makes it possible to suggest that the asymmetric unit is a linear dimer with an H bond between terminal OH groups of the two BHBC molecules. It is also clear that this H-bonded dimer itself cannot be centrosymmetric or close to a center of symmetry, because then all molecular hyperpolarizability tensor components β_{ijk} would be zero so that the crystal would not have an SHG effect regardless of the space group. A reasonable suggestion then would be that within this H-bonded dimer, BHBC molecules are not equivalent, one being H donor and the other H acceptor.

The simulated diffraction patterns for each zone are shown on the RHS of Figs. 2 and 3 whereas the simulated powder pattern is given in Fig. 4. The simulations performed as described previously led to the crystal structure shown in Fig. 5. Fractional coordinates of the simulated model are given in Table II. This model contains the H-bonded dimer with its inertia axes almost exactly parallel to the crystal axes (the longest axis of the dimer is parallel to the crystal b axis).

The crystal structure presents H-bonded layers of BHBC molecules without interlayer H bonding. The H bonding between neighboring asymmetric units within each layer is realized between the hydroxy-group of one molecule and carbonyl group of the other. The obtained packing energy is given below:

Van der Waals energy:	-214.8 kcal/mol
Coulomb energy:	-33.6 kcal/mol
H-bond energy:	-42.0 kcal/mol
Total energy per cell:	-290.4 kcal/mol

C. Quantitative analysis of electron diffraction patterns

Quantitative analysis of electron diffraction data consists of many steps. The procedure adopted for these investigations is indicated below.

Data collection. To overcome the nonlinearity of the CCD sensors for optical density, the photographic calibration

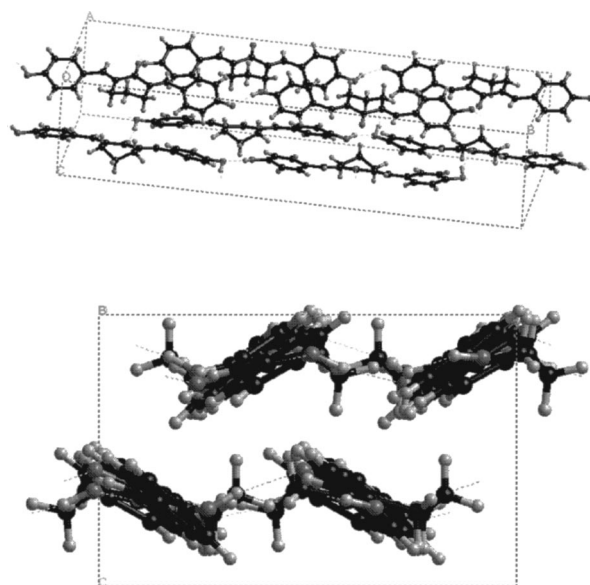


FIG. 5. Crystal structure of BHBC obtained by packing energy minimization procedure.

TABLE I. Experimental and calculated amplitudes and phases of BHBC.

h	k	l	Amplitudes	Phases	h	k	l	Amplitudes	Phases
0	0	2	240.57	51.49	4	0	5	8.38	136.5
0	0	4	33.44	96.79	4	0	6	9.59	3.26
0	0	6	9.77	130.76	4	1	0	42.51	0
0	1	1	3.77	12.08	4	1	1	27	19.22
0	2	0	8.12	180	4	2	0	4.27	0
0	2	2	15.43	165.9	4	2	1	16.67	22.22
0	4	0	24.47	0	4	2	2	3.09	18.43
0	4	2	32.16	140.62	4	3	0	25.86	0
0	4	4	37.37	83.46	4	3	3	5.6	136.66
0	6	0	34.84	0	4	4	0	1.21	0
0	8	0	16.93	0	4	4	1	18.77	31.34
0	8	4	17.53	62.44	4	4	2	12.08	128.64
0	10	0	3.61	180	4	4	3	18.62	87.39
0	12	0	14.49	0	4	4	4	8.74	87.04
0	14	0	8.53	180	4	6	0	20.45	0
0	16	0	3.3	0	4	6	3	5.94	127.65
0	18	0	29.08	180	4	7	0	4.23	180
0	20	0	8.43	0	4	8	0	17.75	0
0	22	0	17.18	0	4	8	1	12.2	16.31
0	24	0	3.35	0	4	9	0	6.35	180
0	26	0	22.57	180	4	10	0	9.73	180
0	30	0	12.51	0	4	12	0	11.84	0
1	1	0	4.48	0	4	13	0	28.35	180
1	1	1	6.88	33.21	4	15	0	21.82	0
1	1	2	5.01	45.2	5	1	0	3.19	180
1	1	4	7.85	74.07	5	1	1	5.06	108.49
1	2	0	26.12	180	5	2	0	16.86	0
1	2	1	24.25	64.11	5	2	1	16.8	89.91
1	2	2	25.45	121.85	5	3	0	5.47	0
1	2	3	15.79	2	5	3	3	1.85	62.07
1	2	4	14.06	81	5	4	2	8.63	157.64
1	3	3	8.36	3.14	5	4	4	8.23	86.22
1	4	2	9.28	90.41	5	5	0	7.91	180
1	5	0	27.05	180	5	5	1	8.46	103.09
1	6	0	44.64	0	5	5	2	7.73	26.66
1	6	3	14.38	50.65	5	5	3	11.01	152.23
1	7	0	1.89	0	5	5	4	9.44	50.53
1	8	0	0.94	180	5	7	0	8.02	180
1	10	5	4.64	3.5	5	8	0	11.65	0
1	11	0	13.46	0	5	9	0	12.52	180
1	14	0	11.59	180	5	12	0	6.93	0
1	15	0	24.84	180	5	13	0	10.24	180
1	16	0	21.93	180	6	0	0	3.42	180
1	18	0	8.48	180	6	0	1	24.83	113.74
1	20	0	13.14	180	6	0	2	9.44	132.55
1	21	0	7.37	180	6	0	3	20.86	173.68
1	26	0	1.09	180	6	0	4	3.44	105.06
1	28	0	11.87	0	6	0	5	11.24	126.08
2	0	0	1.45	180	6	1	1	21.13	70.17
2	0	1	162.8	62.37	6	2	0	0.53	180
2	0	2	119.24	142.55	6	2	1	20.65	57.82
2	0	3	58.19	7.09	6	3	3	14.43	19.31
2	0	4	38.54	162.33	6	4	0	2.1	180
2	0	5	10.46	58.7	6	4	2	8.79	39.04
2	0	6	4.39	127.48	6	5	0	0	0

TABLE I. (*Continued*).

h	k	l	Amplitudes	Phases	h	k	l	Amplitudes	Phases
2	1	0	6.78	0	6	6	1	7.74	48.72
2	1	1	54.69	74.16	6	6	3	2.59	10.36
2	2	1	16.47	24.11	7	1	0	8.94	180
2	2	2	17.44	143.89	7	1	1	8.92	109
2	2	3	9.99	93.46	7	2	0	6.62	0
2	2	4	7.14	86.84	7	2	1	5.28	58.48
2	2	5	0.59	139.99	7	3	0	10.3	0
2	3	3	7.61	56.51	7	3	3	4.58	3.02
2	4	0	0.72	180	7	4	0	3.13	0
2	4	1	52.08	65.44	7	4	2	1.26	169.39
2	4	2	34.72	142.68	7	4	4	4.43	78.12
2	4	3	4.04	62.13	7	10	0	2.6	180
2	4	4	3.67	16.11	7	11	0	7.89	180
2	5	5	13.66	139.81	7	12	0	6.42	0
2	6	3	17.57	163.83	7	13	0	7.1	180
3	1	0	12.49	180	7	14	0	13.91	0
3	1	1	21.64	97.81	7	15	0	8.87	0
3	2	0	8.93	0	7	17	0	10.56	180
3	2	2	2.22	69.27	7	18	0	3.81	180
3	3	0	21.56	0	7	20	0	3.97	180
3	3	1	13.51	114.1	7	21	0	5.19	180
3	3	2	10.75	64.75	7	22	0	3.75	180
3	3	3	8.69	119.67	7	23	0	4.93	180
3	3	4	0.79	106.47	8	0	0	10.08	0
3	4	0	12.35	0	8	0	1	5.37	177.39
3	4	2	6.7	73.09	8	0	2	6.57	35.18
3	6	0	14.24	180	8	0	3	7.81	112.23
3	6	1	15.94	177.47	8	1	0	4.83	180
3	6	2	22.58	147.43	8	2	0	13.26	180
3	6	3	14.74	90.92	8	2	2	4.93	123.03
3	7	0	11.07	180	8	3	0	4.76	180
3	8	0	2.58	180	8	6	0	4.74	180
3	9	0	9.23	0	8	6	3	1.77	120.75
3	10	0	16.82	180	8	7	0	3.33	180
3	11	0	18.44	0	8	9	0	5.18	180
3	13	0	5.73	0	8	11	0	4.83	180
3	15	0	31.77	180	8	13	0	10.48	0
3	16	0	15.8	180	8	17	0	6.51	180
3	17	0	3.86	180	8	18	0	2.91	180
4	0	0	0.46	180	8	20	0	9.85	0
4	0	1	29.8	32.39	8	21	0	5.79	0
4	0	2	33.65	118.67	8	22	0	1.1	0
4	0	3	36.55	83.56	9	1	1	1.66	168.52
4	0	4	30.87	68.47	9	2	1	3.49	64.4

strip (Kodak, 21 strips) was used. Both calibration strip and negative were scanned under the same conditions. Then CCD calibration was performed using the ELD program. The nonlinear response of a negative for different exposure times was determined by obtaining an exposure series for each zone. To decrease the optical noise of CCD sensors which could lead to significant difficulties with the intensity estimation of spots which are rather weak or have high background, scans were taken at least five times for each negative. Then the average values were used for the next step.

Data correction. The R factor between the model and experimental data set were determined for each zone. The data set is normalised by $k = \sum \sqrt{I_{\text{theo}}} / \sum \sqrt{I_{\text{expt}}}$. The different zones were merged by using reflections of medium intensity in the common zone as reference.

The R factor for the complete data set was found to be 26%. This value is reasonable for an uncorrected electron diffraction data set and indicates that the data set is reliable. The temperature factor of the experimental data set was determined to be $B = 1.23 \text{ \AA}^2$ by a Wilson plot which gave a

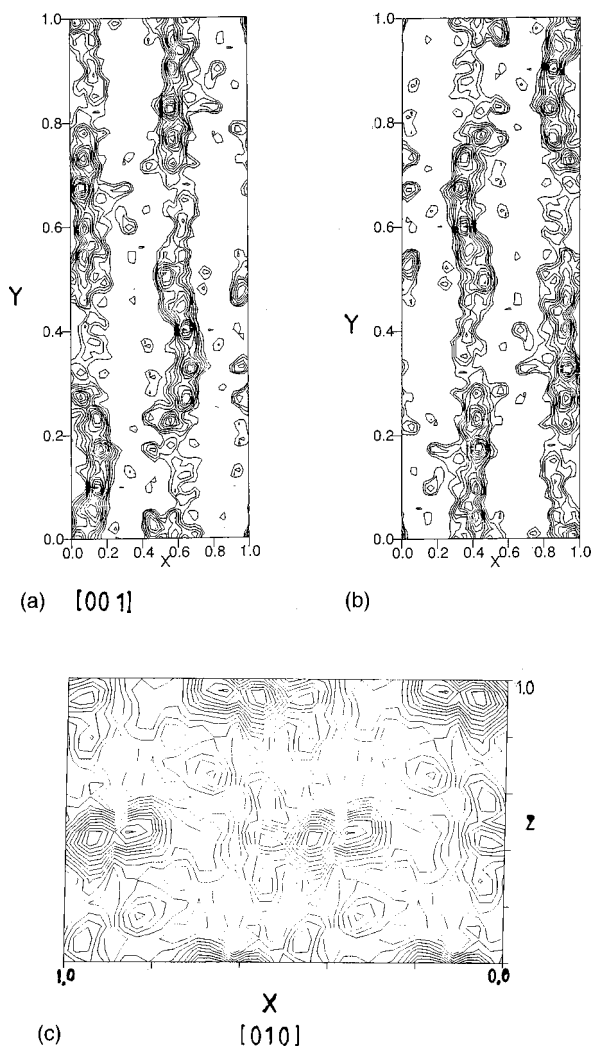


FIG. 6. Centroid maps for BHBC; projection down z (LHS, $z=0-0.5$; RHS, $z=0.5-1$) and projection down y .

good linear relationship. This value is slightly low but still reasonable for organic crystals, especially when compared with the value of 2.5 obtained for the theoretical data set from the model for the same intensity range. In our opinion this is due to the limited number of parameters available for this large unit cell containing 8 molecules. This value thus indicates that the data are reliable. Table I compares experimental with calculated intensities of the determined reflections and shows the calculated phases.

D. Structure solution using maximum entropy and likelihood

The data were normalized as described in Sec. III E. An overall temperature factor of $B=1.2 \text{ \AA}^2$ was computed, and used by the normalization program. Often with electron diffraction data sets B is computed to be negative, which is, of course, physically impossible, and it is a measure of the quality of the data that a positive value is calculated by default. The basis set was defined by fixing the phases of three origin defining reflections with large U -magnitudes (the 2 0 1, 7 21 0 and 4 13 0 reflections with U -magnitudes of 0.28, 0.11, and 0.09 respectively). The enantiomorph was left undefined since the subsequent phasing process defines it *de*

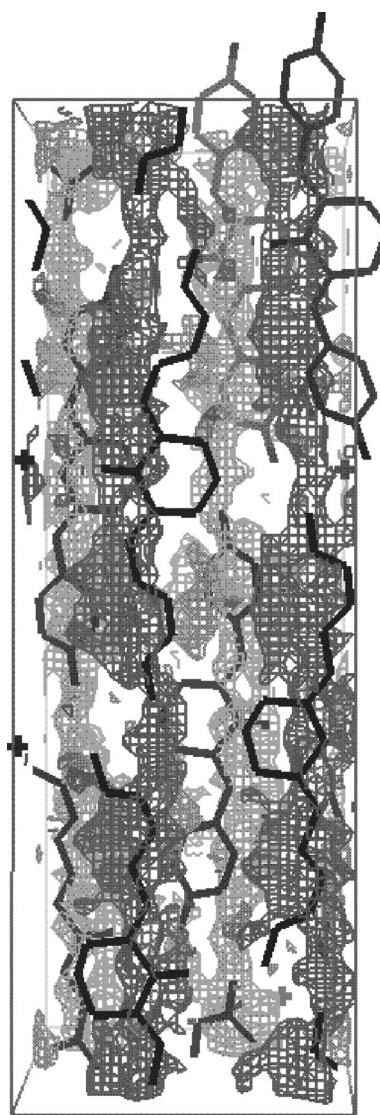


FIG. 7. Centroid maps for BHBC; projection down z with initial fit of the simulated model.

facto. These three reflections defined the root node of the phasing tree. Fifteen reflections were then given permuted phases; six of them were centric (7 15 0, 4 6 0, 3 1 0, 1 28 0, 7 1 0, 7 3 0) and nine acentric (2 0 3, 2 0 2, 2 4 2, 1 2 2, 5 3 3, 0 4 4, 4 0 3, 4 0 6, and 6 0 5). The Golay code was used as a source of phase permutation generating 4096 nodes instead of 2^{24} phase choices, on the second level of the phasing tree. Each of these nodes was subjected to constrained entropy maximization with likelihood evaluation. The algorithm used for entropy optimisation is an iterative one based on exponential modeling;²⁴ LLGs were computed after each cycle and the process terminated at the point of maximum LLG.

The nodes were analyzed via their associated LLGs and the top eight were kept and used to generate centroid maps. Each of these maps is computed using the corresponding basis set reflections plus all the ME extrapolates suitably weighted, provided that the associated Sim weight was >0.1 . They all showed very similar features with electron density running in lines along y in the x - y plane and globs of density in the x - z plane. Figure 6 shows the map that was top ranked

TABLE II. Fractional coordinates of the simulated model.

Atoms	x/a	y/b	z/c	Atoms	x/a	y/b	z/c
C1	0.2888	0.3226	0.4686	C42	0.0255	0.3197	0.9243
C2	0.3817	0.3125	0.3630	C43	0.1262	0.3097	1.0116
H3	0.4211	0.3314	0.3022	H44	0.1688	0.3285	1.0677
C4	0.4155	0.2746	0.3483	C45	0.1630	0.2720	1.0150
H5	0.4768	0.2685	0.2764	H46	0.2296	0.2658	1.0748
C6	0.3591	0.2455	0.4394	C47	0.1020	0.2430	0.9303
C7	0.2729	0.2564	0.5483	C48	0.0076	0.2539	0.8387
H8	0.2346	0.2377	0.6124	H49	-0.0342	0.2353	0.7791
C9	0.2411	0.2937	0.5662	C50	-0.0275	0.2910	0.8317
H10	0.1849	0.2998	0.6475	H51	-0.0897	0.2972	0.7616
C11	0.4006	0.2062	0.4083	C52	0.1477	0.2038	0.9485
H12	0.4754	0.2044	0.3686	H53	0.2250	0.2024	0.9746
C13	0.3474	0.1729	0.4285	C54	0.0952	0.1703	0.9331
C14	0.4126	0.1373	0.3873	C55	0.1651	0.1350	0.9576
C15	0.3607	0.0990	0.4211	C56	0.1132	0.0965	0.9279
C16	0.2381	0.0977	0.4765	C57	-0.0126	0.0946	0.8941
H17	0.2035	0.0746	0.4307	H58	-0.0423	0.0710	0.9424
H18	0.2344	0.0966	0.6035	H59	-0.0256	0.0942	0.7684
C19	0.1701	0.1323	0.4130	C60	-0.0774	0.1283	0.9738
H20	0.0921	0.1305	0.4542	H61	-0.1579	0.1261	0.9463
H21	0.1692	0.1329	0.2858	H62	-0.0690	0.1281	1.1004
C22	0.2253	0.1687	0.4837	C63	-0.0299	0.1655	0.8990
H23	0.1825	0.1907	0.4424	H64	-0.0706	0.1869	0.9505
H24	0.2215	0.1685	0.6107	H65	-0.0431	0.1660	0.7735
C25	0.4255	0.0684	0.3944	C66	0.1813	0.0662	0.9388
H26	0.4990	0.0735	0.3554	H67	0.2569	0.0717	0.9654
C27	0.3985	0.0274	0.4174	C68	0.1551	0.0252	0.9150
C28	0.4647	0.0017	0.3208	C69	0.2295	-0.0006	0.9958
H29	0.5232	0.0110	0.2505	H70	0.2923	0.0087	1.0567
C30	0.4449	-0.0374	0.3277	C71	0.2115	-0.0398	0.9870
H31	0.4907	-0.0540	0.2633	H72	0.2627	-0.0564	1.0406
C32	0.3564	-0.0522	0.4308	C73	0.1168	-0.0545	0.8979
C33	0.2988	-0.0264	0.5339	C74	0.0505	-0.0286	0.8092
H34	0.2453	-0.0355	0.6137	H75	-0.0080	-0.0376	0.7381
C35	0.3169	0.0121	0.5237	C76	0.0670	0.0099	0.8215
H36	0.2723	0.0284	0.5913	H77	0.0168	0.0263	0.7644
O37	0.2364	0.3571	0.4659	O78	-0.0120	0.3558	0.8979
H38	0.1690	0.3520	0.4070	H79	-0.0836	0.3556	0.9490
O39	0.5082	0.1396	0.3216	O80	0.2648	0.1376	1.0065
O40	0.3368	-0.0898	0.4608	O81	0.0802	-0.0912	0.9096
H41	0.4059	-0.1010	0.4326	H82	0.1473	-0.1051	0.9026

in terms of LLG analysis. Some maps displayed less detail than this. Since the effective resolution of the data is ca. 1.5 Å, and because the data and phases are incomplete and subject to error, only the molecular outline is visible, and, to impose atomicity, model building was then used in which the molecular model was superimposed on the density rotating as necessary around the bonds which had the necessary torsional freedom. (It is worth emphasizing that this is the first point where the model was used in the structure determination process.) This method is used routinely in protein crystallography, for example, but is much less common in the

small molecule crystallographic environment. The initial fit of the molecule to the density is shown in Fig. 7, and it can be seen that this accounts for most of the features of the centroid map. At this point the structure was ready for least-squares crystallographic refinement. The entire calculation was routine, and, using a network cluster of UNIX workstations, took less than 2 hours cpu time in total.

A third level of the phasing tree was also computed to see if any enhancement of resolution could be found in the electron density, but the maps were broadly similar to those of the second level and no easier to interpret.

TABLE III. Calculated values of the components of α tensor of a unit cell per molecule, local-field factors, f_I , and refractive indices, n_I , in the crystal coordinate systems.

	6-31G(+sp,+sd)			
	PM-3 static	static	$\lambda = 1064$ nm	$\lambda = 532$ nm
$\alpha_{XX}, \text{\AA}^3$	44.9	55.2	55.7	57.4
$\alpha_{YY}, \text{\AA}^3$	112.7	131.0	135.8	155.1
$\alpha_{ZZ}, \text{\AA}^3$	17.4	40.6	40.9	41.8
f_X	1.315	1.417	1.422	1.441
f_Y	2.505	3.316	3.624	5.779
f_Z	1.102	1.276	1.279	1.287
n_X	1.395	1.500	1.505	1.524
n_Y	2.348	2.819	2.979	3.916
n_Z	1.143	1.352	1.355	1.364

E. Quantum-mechanical calculations of the molecular polarizabilities and their relationships to macroscopic NLO coefficients of the BHBC crystal

In this section, macroscopic NLO coefficients, d_{IJK} , are estimated using Eq. (1) with both the PM-3 as well as the *ab initio* calculated values of molecular tensor components of linear polarizability α and PM-3 calculated values of quadratic polarizability β .

Using the Lorenz-Lorentz relations:

$$(n_I^2 - 1)/(n_I^2 + 2) = (4/3)\pi(N/V)\alpha_{II}, \quad (6)$$

the local-field factors, f_I , in Eq. (1) are

$$f_I = (n_I^2 + 2)/3 = 1/[1 - (4/3)\pi(N/V)\alpha_{II}], \quad (7)$$

where α_{II} are the diagonal components of the α tensor of the unit cell per molecule.

The molecular α tensors calculated by both the PM-3 and 6-31G(+sp,+sd) *ab initio* methods for the asymmetric unit (H-bonded BHBC dimer) of the crystal were reduced to the crystal frame to give the α_{II} components of the resultant α tensor of the unit cell per molecule. The results are summarized in Table III (for the *ab initio* data, frequency-dependent values are also presented). It should be noted that for the particular arrangement of the BHBC molecules in the unit cell determined here the following relationship between the molecular (x,y,z) and crystal (X,Y,Z) axes holds: $x=Y$, $y=X$, $z=Z$.

As seen from Table III, the PM-3 method underestimates linear polarizability tensor components, especially α_{ZZ} . *Ab initio* data presented in Table III show that frequency dependence influences considerably only the α_{YY} value and the corresponding local-field factor, f_Y .

The largest component of the molecular β tensor for the dimeric asymmetric unit is β_{xxx} , characterizing the intramolecular charge transfer along the molecular longest x axis of the asymmetric unit. Therefore this H-bonded BHBC dimer itself might be considered as a one-dimensional NLO chromophore. However, the observed NLO effect of the BHBC crystal powder cannot be due to β_{xxx} because the molecular x axis is exactly perpendicular to the crystal 2_1 axis (c axis), leading to cancellation of the one-dimensional contribution.

Similarly, two-dimensional contributions due to β_{xyy} and β_{yxx} vanish upon taking into account the crystal symmetry because the molecular xy plane is exactly perpendicular to the crystal 2_1 axis. Therefore, the BHBC crystal NLO properties can only be related to two-dimensional charge transfer in yz - and xz -molecular planes parallel to the crystal c axis, the only relevant nonzero β component being β_{zxx} . For this reason, a two-dimensional model, as proposed by Zyss,² was used for this crystal structure. Taking then into account the permutation between the molecular x and y axes (the longest x axis of the H-bonded BHBC dimer in the unit cell is parallel to the Y axis of the crystal frame, while it would be along the X axis of the crystal frame according to the axes convention used by Zyss,² $b_{ZYY} = \beta_{zxx} = 1.0 \times 10^{-30}$ esu, according to the PM-3 estimation.

Thus, the estimated d_{ZYY} coefficient is PM-3:

$$d_{ZYY} = (N/V)f_Z(f_Y)^2 b_{ZYY} = 8.8 \times 10^9 \text{ esu} = 3.67 \text{ pm/V};$$

ab initio (static local-field factors):

$$d_{ZYY} = (N/V)f_Z(f_Y)^2 b_{ZYY} = 17.9 \times 10^{-9} \text{ esu} = 7.45 \text{ pm/V};$$

ab initio (frequency-dependent local-field factors):

$$d_{ZYY} = (N/V)f_Z(2\omega, \lambda = 532 \text{ nm})f_Y^2(\omega, \lambda = 1064 \text{ nm})b_{ZYY} \\ = 21.5 \times 10^{-9} \text{ esu} = 8.97 \text{ pm/V}.$$

V. CONCLUSIONS

In this paper it has been shown that by combining methods of structure determination with quantum-mechanical calculations it is possible to calculate the nonlinear optical coefficients for a type of two-dimensional molecule.

Both semiempirical and *ab initio* calculations gave rise to gas phase molecular conformations with a symmetry plane passing through the C=O double bond of the BHBC molecule perpendicular to its longest axis. This molecular gas phase symmetry is distorted in the crystal state due to the formation of H bonds, one of the two terminal OH groups of each BHBC molecule being H donor and the other H acceptor.

It should be noted that the *ab initio* gas phase geometry almost exactly reproduces the extended BHBC conformation in the crystal state, while the PM-3 method predicts highly folded gas phase conformation. The reason of the PM-3 failure to reproduce the correct conformation is, probably, an incorrect description of the balance between the π conjugation along the molecule (favoring a flat and extended conformation) and steric repulsion between the protons of phenyl and cyclohexane fragments (favoring a strongly folded conformation). Among the available semiempirical methods (MNDO, AM1, PM-3), the PM-3 method is known to be the least disadvantageous with respect to this balance. However, in the particular case studied here it is still not satisfactory.

In order to determine the orientation of the molecule with respect to the crystal axes, electron diffraction was used. A routine application of this method is not possible because electron intensities are severely affected by dynamical and secondary scattering.⁴⁵ In addition to this, quantitative analysis of the data depends on the non linear properties of the

emulsion, the response of the CCD chip and on the soft ware used to evaluate the intensities. Despite these problems, it was shown that reasonable R factors can be obtained and a correct low resolution structure determined.

Packing energy calculations as described previously^{5,7a,8,10} were then used to refine the structure and obtain atomic positions. On the basis of these positions, the values of the molecular α - and β -tensor components could be calculated and related to the crystal properties. The symmetry of the crystal is such that many components of the hyperpolarizability tensor virtually cancel.

The differences between the PM-3 and *ab initio* values of α -tensor components for the H-bonded BHBC dimer (asymmetric unit of the BHBC crystal) lead to the underestimation of the d_{ZYY} value by the PM-3 method compared to *ab initio* by a factor of only 2–2.5. This cannot be considered as a bad qualitative estimation by the PM-3 method although the necessity of an *ab initio* approach in the case of this molecule for better estimates is revealed. The discrepancy between the PM-3 and *ab initio* α_{II} values is probably due to an incorrect

semiempirical description of σ -electron contributions to the α -tensor components. The π -electron contributions are usually described satisfactorily by the semiempirical methods. In particular, molecular β -tensor components, dependent mainly on the π -electron contributions for π -conjugated molecules, are well reproduced by the PM-3 method.⁴⁶

Independently the structure was determined by using maximum entropy methods which were specifically developed for crystallographic applications.^{24,47} Because of the limited number of reflections obtained by electron diffraction from beam sensitive samples, the resolution of the potential maps was limited. However, the maps clearly reflect the structure determined by molecular modeling combined with quantum-mechanical calculations. The model shows that layers of H-bonded momolecules were obtained due to the formation of dimers.

ACKNOWLEDGMENT

We gratefully acknowledge financial support for this work by the Deutsche Forschungsgemeinschaft.

*Author to whom correspondence should be addressed.

[†]Permanent address: Institute of Macromolecular Compounds of Russian Academy of Sciences, Bolshoi prospect 31, 199004 St. Petersburg, Russia.

¹T. Tomono, L. S. Pu, T. Knoshita, K. Sasaki, and S. Umegaki, *J. Phys. D* **26**, B217 (1993).

²J. Zyss and J. L. Oudar, *Phys. Rev. A* **26**, 2028 (1982).

³I. Ledoux, J. Zyss, J. S. Siegel, J. Brienne, and J. M. Lehn, *Chem. Phys. Lett.* **172**, 440 (1990).

⁴I. G. Voigt-Martin, M. Schumacher, and R. Garbella, *Macromolecules* **25**, 961 (1992).

⁵I. G. Voigt-Martin, D. H. Yan, R. Wortmann, and K. Elich, *Ultramicroscopy* **57**, 29 (1995).

⁶I. G. Voigt-Martin, Z. X. Zhang, D. H. Yan, A. Yakimanski, R. Wortmann, R. Matschiner, P. Krämer, C. Glania, and N. Detzer, *Colloid Polym. Sci.* **275**, 18 (1997).

⁷(a) I. G. Voigt-Martin, GaO Li, A. Yakimanski, J. J. Wolff, and H. Gross, *J. Phys. Chem. A* **101**, 7265 (1997); (b) I. G. Voigt-Martin, Li Gao, A. Yakimanski, G. Schulz, and J. J. Wolff, *J. Am. Chem. Soc.* **118**, 12 830 (1996).

⁸A. Yakimanski, I. G. Voigt-Martin, U. Kolb, G. N. Matveeva, and A. V. Tenkovtsev, *Acta Crystallogr., Sect. A: Found. Crystallogr.* **A53**, 603 (1997).

⁹I. G. Voigt-Martin, D. H. Yan, C. Gilmore, K. Shankland, and G. Bricogne, *Ultramicroscopy* **56**, 271 (1994).

¹⁰I. G. Voigt-Martin, D. H. Yan, A. Yakimanski, D. Schollmeyer, C. J. Gilmore, and G. Bricogne, *Acta Crystallogr., Sect. A: Found. Crystallogr.* **A51**, 849 (1995).

¹¹I. G. Voigt-Martin, Z. X. Zhang, U. Kolb, and C. Gilmore, *Ultramicroscopy* **68**, 43 (1997).

¹²J. J. P. Stewart, *J. Comput. Chem.* **10**, 209 (1989).

¹³J. J. P. Stewart, MOPAC 6.0, A General Purpose Molecular Orbital Package, QCPE (1990).

¹⁴R. G. Parr and W. Yang, *Density-Functional Theory of Atoms and Molecules* (Oxford University Press, Oxford, 1989).

¹⁵R. Ahlrichs, M. Bär, M. Häser, H. Horn, and C. Kölmel, *Chem. Phys. Lett.* **162**, 165 (1989).

¹⁶(a) A. D. Becke, *Phys. Rev. A* **38**, 3098 (1988); (b) J. P. Perdew, *Phys. Rev. B* **33**, 8822 (1986).

¹⁷A. Schäfer, H. Horn, and R. Ahlrichs, *J. Chem. Phys.* **97**, 2571 (1992).

¹⁸H. A. Kurtz, *Int. J. Quantum Chem.* **24**, 791 (1990).

¹⁹M. A. Spackman, *J. Phys. Chem.* **93**, 7594 (1989).

²⁰J. Cowley, *Electron Diffraction Techniques* (Oxford Science Publications, Oxford, 1992), Vol. 1.

²¹D. Dorset, *Structural Electron Crystallography* (Plenum, New York, 1995).

²²U. Kolb, H. Kothe, I. G. Voigt-Martin, and U. Kolb (unpublished).

²³S. Hovmöller, *Ultramicroscopy* **41**, 121 (1992).

²⁴G. Bricogne, *Acta Crystallogr., Sect. A: Found. Crystallogr.* **A40**, 410 (1984).

²⁵G. Bricogne and C. J. Gilmore, *Acta Crystallogr., Sect. A: Found. Crystallogr.* **A46**, 284 (1990).

²⁶C. J. Gilmore, G. Bricogne, and C. Bannister, *Acta Crystallogr., Sect. A: Found. Crystallogr.* **A46**, 297 (1990).

²⁷C. J. Gilmore, K. Henderson, and G. Bricogne, *Acta Crystallogr., Sect. A: Found. Crystallogr.* **A47**, 830 (1991).

²⁸C. J. Gilmore, L. D. Marks, D. Grozea, C. Collazo, E. Landree, and E. R. Twisten, *Surf. Sci.* **381**, 77 (1997).

²⁹C. J. Gilmore, W. V. Nicholson, and D. L. Dorset, *Acta Crystallogr., Sect. A: Found. Crystallogr.* **A52**, 937 (1996).

³⁰C. J. Gilmore and G. Bricogne, *Methods Enzymol.* **277**, 65 (1997).

³¹C. J. Gilmore, *Acta Crystallogr., Sect. A: Found. Crystallogr.* **A52**, 561 (1996).

³²C. J. Gilmore, *J. Appl. Crystallogr.* **17**, 42 (1984).

³³G. Bricogne, *Acta Crystallogr., Sect. D: Biol. Crystallogr.* **D49**, 37 (1993).

³⁴G. Bricogne, *Methods Enzymol.* **276**, 424 (1997).

³⁵C. J. Gilmore, W. Dong, and G. Bricogne, *Acta Crystallogr. Sect. A: Found. Crystallogr.* (to be published).

³⁶F. J. MacWilliams and N. J. A. Sloane, *The Theory of Error-Correcting Codes* (North-Holland, Amsterdam, 1977).

³⁷R. Hill, *A First Course in Coding Theory* (Oxford University Press, Oxford, 1993).

³⁸M. J. E. Golay, *Proc. IRE* **37**, 23 (1949).

³⁹J. Leech, *Can. J. Math.* **19**, 251 (1967).

- ⁴⁰K. Shankland, C. J. Gilmore, G. Bricogne, and H. Hashizume, *Acta Crystallogr., Sect. A: Found. Crystallogr.* **A49**, 493 (1993).
- ⁴¹G. A. Sim, *Acta Crystallogr.* **12**, 813 (1959).
- ⁴²C. J. Gilmore and W. V. Nicholson, *Trans. Am. Crystallogr. Assoc.* **30**, 15 (1994).
- ⁴³J. Gjønnnes, V. Hansen, P. Runde, Y. F. Cheng, K. Gjønnnes, C. J. Gilmore, and D. Dorset, *Acta Crystallogr., Sect. A: Found. Crystallogr.* **A54**, 306 (1998).
- ⁴⁴M. Loos-Wildenauer, S. Kunz, I. G. Voigt-Martin, A. Yakimanski, E. Wischerhoff, R. Zentel, C. Tschierske, and M. Müller, *Adv. Mater.* **7**, 170 (1995).
- ⁴⁵D. Dorset, *Structural Electron Crystallography* (Plenum, New York, 1995).
- ⁴⁶H. A. Kurtz, J. J. P. Stewart, and K. M. Dieter, *J. Comput. Chem.* **11**, 82 (1990).
- ⁴⁷C. Gilmore, K. Shankland, and G. Bricogne, *Proc. R. Soc. London, Ser. A* **442**, 97 (1993).